GFDM Zero Forcing Equalizer for Large Doppler Shift in Correlated Double Ring Channel Models

Wahyu Pamungkas[1,*], Anggun Fitrian Isnawati[1], and Haryadi Teguh Pribadi[2]

[1] Institut Teknologi Telkom Purwokerto, Purwokerto 53147, Indonesia
[2] PT. Telkomsat, Indonesia
*Correspondence: wahyu@ittelkom-pwt.ac.id (W.P.)

***Abstract*—The nature of wireless communication channels evolves throughout time. Depending on the channel model, wireless communication channels can also be affected by a number of key factors. In the Correlated Double Ring (CDR) wireless channel model, the channel gain parameters are affected by the movement of vehicles on the transmitter and receiver sides as well as the amount of scatterers surrounding the transmitter and receiver. When bits are transmitted across the CDR channel using a Generalized Frequency Division Multiplexing (GFDM) multi-carrier system, the received bit will be degraded as a result of Doppler shift and multipath. To circumvent this, we use a Zero Forcing (ZF) equalizer to correct the erroneous bits on the receive side. In this study, we simulate data bits transmitted via a CDR channel at various speeds, ranging from low speed to high speed, using a GFDM multicarrier system. The ZF equalization method that we propose to overcome the higher Doppler frequency on a high-speed CDR channel of 95 m/s with the scatterer of 8 has been demonstrated to increase Bit Error Rate (BER) performance in comparison to the emergence of a ZF equalization scheme. In order to counteract the vast number of up to 16 multipaths on CDR channels, the ZF equalization approach can improve the BER performance at 95 m/s when compared to when it is not employed. On the Rician CDR channel, the ZF equalization algorithm can efficiently overcome the highly significant Doppler effect and multipath fading.**

***Keywords*—correlated double ring, wireless channel model, Doppler shift, GFDM, zero forcing**

I. Introduction

Wireless communication system applications that require user mobility and move up to high speed are commonly known as vehicular-based communication systems. This vehicular communication system is now developing, with reference to several technical standards that have been developed. Among the technology standards that govern this vehicular communication system is the standardization of Dedicated Short-Range Communications (DSRC) [1–4]. This standard regulates the communication system between vehicles, and vehicles with telecommunications infrastructure that can move with high mobility and a range of up to 500 meters with a frequency of 5.9 GHz [5]. Another vehicular communication standard is applied to cellular technology, which is regulated by the 3rd Generation Partnership Project (3GPP) with Vehicle to Everything (V2X) technology [6–10]. This technology has been applied from 4G technology or long-term evolution (LTE) to 5G technology.

Generally, each of these standardizations of vehicular communication technology employs a unique channel model that differs from other wireless communication channels. The most important characteristic that distinguishes vehicle communications from other wireless systems is their distinct channel propagation characteristics [11]. Vehicle communication is differentiated by a dynamic environment, high mobility, and relatively low antenna heights on the communicating entities [12]. As a result of these factors, vehicular propagation and channel modeling are especially difficult to realize.

Due to the special characteristics of vehicle channels mentioned above, many existing mobile channel models, while widely utilized for cellular systems, are often unsuitable to use in vehicular systems. For instance, a large change in signal propagation behavior could be caused by differences in the relative height of the transmitter and receiver antennas. Furthermore, the design of user speed in cellular communication systems frequently anticipates the movement of users at slow to medium speeds only. This is in contrast to the speed of a vehicular communication system, which can travel at high speeds.

The channel model of the vehicular communication system has been studied previously by [5, 11–15]. The channel modeling approach in vehicular communication system is divided into Geometry-Based Deterministic (GBD), Geometry-Based Stochastic (GBS), and Non-Geometry-Based (NGS). The GBD models include relevant simulation-area objects and calculate channel statistics in a fully deterministic manner. The GBS models calculate channel statistics based on statistics extracted from measurements or simulated data, while accounting for environmental geometry. NGS models generate channel statistics in a completely stochastic manner because both geometrical qualities and channel statistics are created stochastically.

Manuscript received August 29, 2022; revised September 29, 2022, accepted December 20, 2022

The Correlated Double Ring (CDR) channel model, which was created by [16] and validated by [17], is one of channel-modeling type used in this study. This CDR channel model begins with mobile-to-mobile communication, which accommodates transmitter and receiver movement and takes into account the presence of multipath, which is in two rings on the transmitter and receiver sides. This multipath has the same amount of mutual correlation between the transmitter and receiver sides but it is static. Previous studies by the author reviewed the use of CDR channels for vehicular communication systems [18]. They modeled the power spectral density of CDR channels combined with multi-carrier Orthogonal Frequency Division Multiplexing (OFDM) [19] and the detection of Doppler spread values from the Doppler spectrum of CDR channels [20] as well as an investigation of the effect of angle of arrival (AoA) on the CDR channel [21].

Due to the mobility of the transmitter and receiver, the CDR channel is characterized by a rather high Doppler shift value. In addition, the presence of a large number of multipaths in the area surrounding the transmitter and receiver produces a significant delay spread. Multipath propagation becomes a distinct gain channel section that is merged with the piece of the propagation model that experiences a line of sight (LOS). This results in the occurrence of Rayleigh and Rician channel gain. The CDR channel's propagation characteristics have been changed to Rayleigh on both sides, and it has been used as a new channel model [22].

Previously, Pamungkas *et al*. [18] and Isnawati *et al.* [19] demonstrated the use of CDR channels integrated with a multi-carrier system in a communication system. However, previous research has not focused on mitigating the effects of the Doppler shift and multipath from the CDR channel. If these two issues are not addressed, Doppler spread and delay spread phenomena will occur, resulting in inter-symbol interference (ISI) and inter-carrier interference (ICI) [23]. Furthermore, if this happens, the system's quality of service will suffer as a result of the poor BER value.

It has been proven in previous research that the generalized frequency division multiplexing (GFDM) system can improve the 5G network system by addressing the shortcomings of OFDM, because GFDM offers benefits that are absent in OFDM. The physical layer must satisfy a large number of demanding requirements to support the anticipated 5G network service. These services can be categorized into application scenarios, each with specific requirements for 5G network management. GFDM can be tailored to meet the specialized requirements of various 5G scenarios [24]. GFDM has several benefits, including the ability to overcome the disadvantages of OFDM, specifically out-of-band (OOB) radiation controlled by pulse shaping filters applied to each subcarrier. GFDM also employs a cyclic prefix (CP) to combat ISI on multipath channels. The simple GFDM structure facilitates synchronization and reduces power consumption [25].

In the majority of cases, efforts have been made in the past to counteract the Doppler effect that occurs on a wireless communication channel by employing the zero forcing (ZF) equalization method. The ZF equalization method is utilized in the research that is carried out by [26]. This method is applied to multi-carrier OFDM with channel circumstances that are double selective channels. This research is comparable to the one that was carried out in this paper. However, the multi-carrier and the type of channel used were different. Another investigation about the use of zero forcing equalization as a means of overcoming ISI was carried out by [27], with the primary focus being on the simplification of zero forcing at increasingly higher levels. This investigation was carried out on the receiving end of a Digital Video Broadcasting Terestrial (DVB-T) communication system using a multipath communication channel type. There was no Doppler effect present throughout any part of the investigation. DVB-T2 is a European ETSI standard published for the first time in 2009. It increases the capacity to 50 Mbit/s and offers greater system design flexibility compared to its predecessor. The same researcher conducted additional study on the zero forcing equalizer [28] by focusing on ICI mitigation with the utilization of iteration detection on the Wi-Max communication system at a maximum speed of 300 kilometers per hour. The research provided in this publication differs from all of these other studies in terms of the multi-carrier and the type of channel that was utilized.

The Doppler effect and multipath fading on CDR channels that are integrated with the GFDM multi-carrier system for vehicular communication are the motivations that we are conducting this research. Our goal is to develop a strategy that can mitigate those effects. In order to mitigate the Doppler effect and multipath fading, the ZF equalizer is implemented. The purpose of this study is to merge CDR channels with multi-carrier GFDM, a technique that has the potential to be utilized in the future 6G cellular communication systems. The contributions of this research including the process of integrating the CDR channel with multi-carrier GFDM utilizing the 16-Quadrature Amplitude Modulation (QAM), as well as the process of mitigating Doppler effects and CDR channel multipath utilizing the ZF equalizer. Both of these processes are described below. The validity of this integration's conclusion can be scrutinized through a theoretical comparison of the coincidence of mistake using 16-QAM. According to our findings, there has not been any other work that has integrated the CDR channel with the multi-carrier GFDM and reduced the Doppler effect by employing the zero force equalization method.

The remaining part of this paper is divided into four sections. Section I is Introduction and Section II discusses the research method, which includes the proposed CDR channel model, GFDM multi-carrier, 16-QAM modulation,

and ZF equalizers. Section III contains the results and discussion session, while Section IV provides the conclusions.

II. Proposed Method

The method that we suggest in this research is derived from the flowchart that can be found in Fig. 1. The CDR channel model, which was established in earlier research and is used in this study, is first validated by employing autocorrelation and probability distribution functions, and then used in the study itself. Next, we validate the BER value without utilizing zero forcing by integrating the channel model with the multi-carrier GFDM-OQAM. We determined that it was correct by contrasting the BER values that were achieved without the use of zero forcing with the theoretical BER values that were associated with the Rayleigh and Rician channels. After performing the steps described above, we then carry out an equalization using zero forcing. The results of this equalization are then compared with the BER value obtained prior to the application of zero forcing, as well as with the BER value calculated theoretically by using of the Rayleigh and Rician channels.

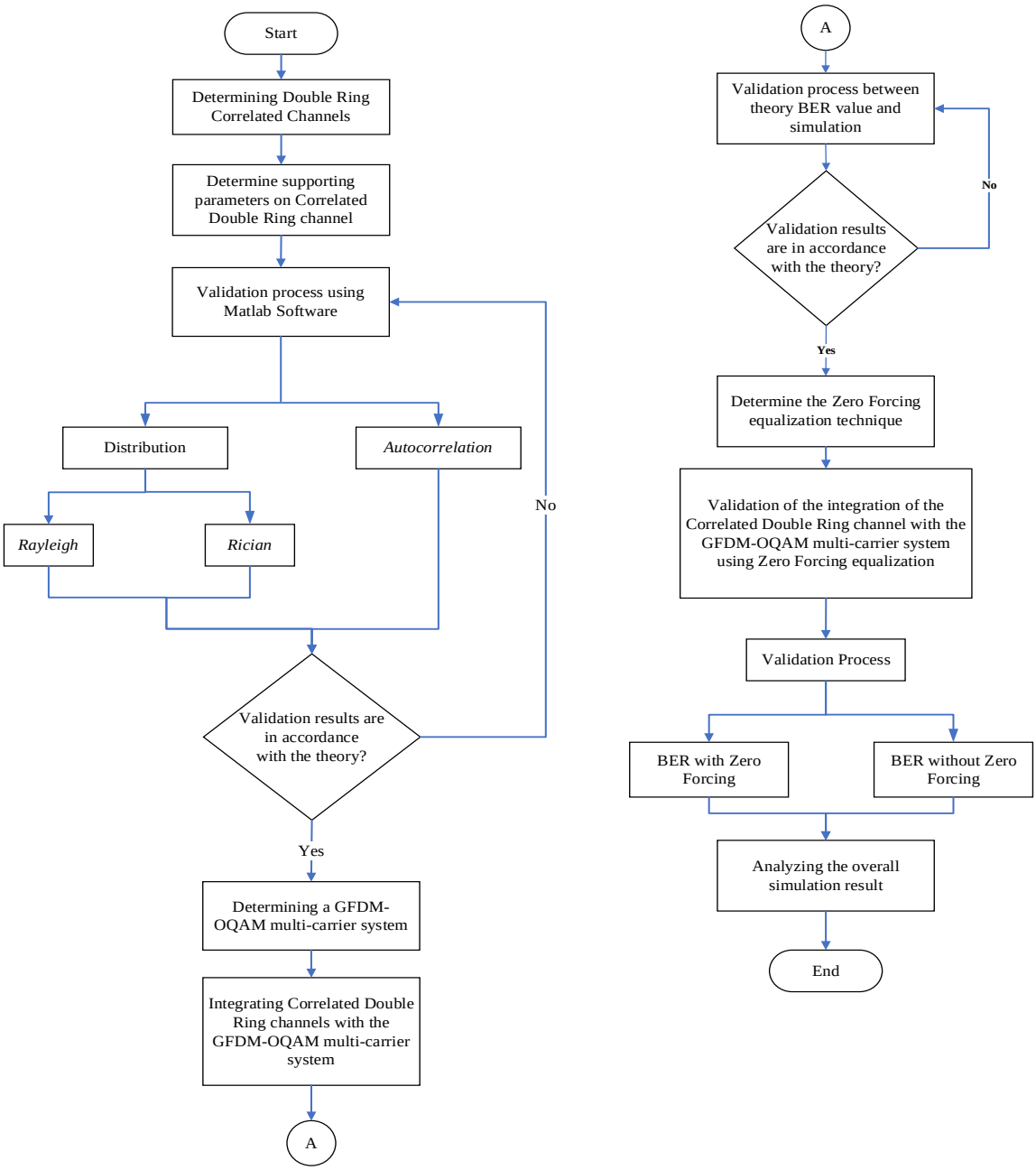

Figure 1. Flowchart of the proposed method.

A. The CDR Channel Model

The channel model used in this paper is entirely based on the findings of [16]. Fig. 2 depicts the CDR channel, which includes a transmitter (Tx) that can move at speed V_1 at an angle θ and a receiver (Rx) that can move at speed V_2 at an angle ψ. It is assumed that scatterers have the same number of transmitters and receivers as the transmitter and

receiver that are scattered around the circle. This scatterer divides signal propagation from the transmitter into two scenarios: propagation that hits the scatterer on the transmitting circle side, moves to the scatterer on the receiving circle side, and finally enters the receiver. The following scenario is Line of Sight (LOS) propagation from the transmitter (Tx) to the receiver (Rx). Line-of-sight propagation is a property of electromagnetic radiation and acoustic wave propagation, which implies that waves travel in a straight line from the source to the receiver.

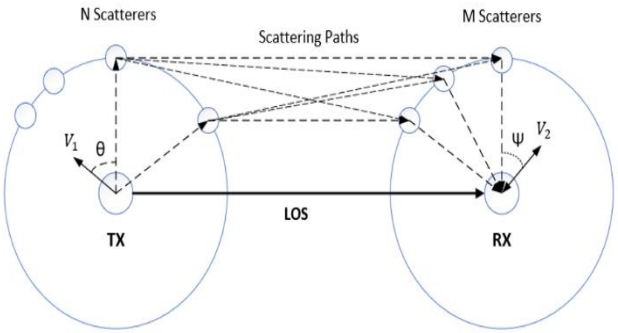

Figure 2. Multipath conditions in the CDR channel model.

The resultant geometry is depicted in Fig. 2 and is the consequence of the movement of the transmitter and receiver on the CDR channel. The transmit angle θ_{send} is produced by the transmitter's movement in relation to the horizontal axis, and the θ_{diff} angle is produced by the velocity vectors V_1 and V_2. Additionally, the combined velocity of V_1 and V_2 will result in V_3, which will then cause the CDR channel to create the Dopper shift (f3). The angle produced by velocity directions V_1 and V_3 is referred to as θ_{3diff} in the following.

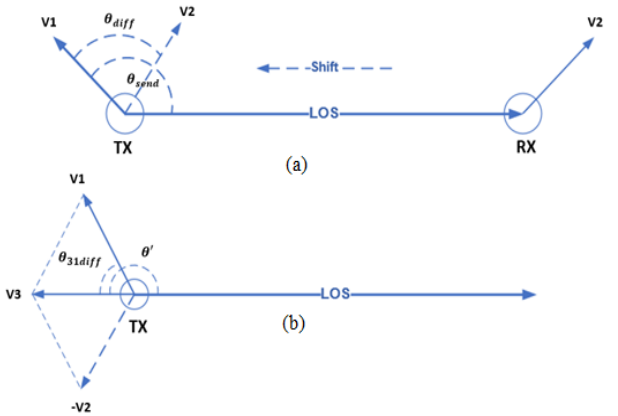

Figure 3. (a) Geometry-Based on the CDR channel model. (b) Resultant speeds of V1 and V2.

The value of V_3 in Fig. 3 can be defined from several previously mentioned angles, namely [16]:

$$V_3 = \sqrt{(V_1.cos(\theta_{diff}) - V_2)^2 + (V_1.sin(\theta_{diff}))^2} \quad (1)$$

The value of θ' is the angle between V_3 and the LOS component toward the receiver with the following values [16]:

$$\theta' = \theta_{send} + \theta_{31diff} \quad (2)$$

where the value of θ_{diff} is the angle between the vectors V_1 and V_2. Notation θ_{send} is the angle between vector V_1 and the LOS component, and the angle between vectors V_1 and V_2 velocity direction is as follows [17]:

$$\theta_{31diff} = cos^{-1}\left(\frac{V_1^2 + V_3^2 - V_2^2}{2V_1V_3}\right) \quad (3)$$

The LOS component of mobile-to-mobile communication can be expressed by the following Eq. (4), [16]:

$$LOS = \sqrt{K}\exp\left[j\left(2\pi f_3 t\cos(\theta') + \emptyset_0\right)\right] \quad (4)$$

The LOS component consists of the K parameter, which indicates the ratio value between specular power and scattering power, the f_3 value, which is the Doppler frequency due to movement with velocity V_3, and angle ϕ_0, which is the initial phase during the interval (-π, π). The f_3 value is obtained from [16]:

$$f_3 = \frac{V_3}{\lambda} \quad (5)$$

where λ is the wavelength value.

B. The CDR Rayleigh Channel Model

The propagation model for the CDR channel that takes into account LOS and Non-LOS (NLOS) situations has already been stated. This can be described using a Rayleigh propagation model with channel gain values for NLOS conditions [17]:

$$Y(t) = \sqrt{\frac{1}{N\,M}}\left\{\sum_{n,m=1}^{N,M} exp\,(j(2\pi f_1\,tcos(\alpha_n) + 2\pi f_2 tcos(\beta_m) + \emptyset_{nm}))\right\} \quad (6)$$

The components that make up the channel gain with Rayleigh propagation above consist of N and M, which are the number of scatterers on the both position, f_1 and f_2, which are Doppler frequencies on the transmitting and receiving sides, and ϕ_{nm} is an independent random phase, which is uniformly distributed over a range of angles (-π,π). The values of α_n and β_m in the previous formulas can be determined by [17]:

$$\alpha_n = \frac{2n\pi - \pi + \theta_n}{4N} \quad (7)$$

$$\beta_m = \frac{2(2m\pi - \pi + \psi_{m)}}{4M} \quad (8)$$

I. The CDR Rician Channel Model

The Rician CDR channel allows signal propagation from transmitter to receiver while dealing with multipath and LOS conditions. As a result, the constituent components of this Rician CDR channel are a Rayleigh CDR channel coupled with a LOS component. The channel gain of the Rician fading CDR channel is as follows Eq. 9, [17]:

$$Z(t) = \frac{\mathrm{Y(t)} + \sqrt{\mathrm{K}}\exp\left(\mathrm{j}(2\pi f_3\, t\cos(\theta^{'}) + \phi_0)\right)}{\sqrt{1+K}} \qquad (9)$$

The parts that make up the channel gain of the Rician CDR channel consist of K, which is the ratio value between specular power and scattering power, f_3, which is the Doppler frequency due to the movement of the transmitter and receiver, and ϕ_0, which is the initial phase. In this study, the setting of the CDR channel with the various variables used is set in Table I.

TABLE I. DEFINITION OF THE CDR CHANNEL VARIABLE

No	Variable	Definition	Value / Quantity
1	$V_1 = V_2$	Vehicle speed as transmitter and receiver	5 m/s, 20 m/s, and 95 m/s
2	M, N	The number of scatterers on the transmitter and receiver sides	8 or 16
3	fc	Carrier frequency	5.8×10^9 Hz
4	K	Comparison of received power and reflected power	1
5	θ_n, Ψ_m	Arrival angle and departure angle	A random integer value between -180° – 180° with a uniform distribution
6	θ_{send}	The angle between the direction of movement of the transmitter vehicle and the horizontal line	30°
7	θ_{31diff}	The angle between the direction of the receiver vehicle and the horizontal line	60°
8	fs	Sampling frequency	80 Hz

C. The GFDM Multi-Carrier

GFDM is a recently proposed block-filtered multi-carrier modulation scheme for future wireless communication systems. The GFDM is a waveform candidate for the next wireless technology that adopts the OFDM principle in which the GFDM signal is constructed from the sum of tones. The GFDM is based on independent block modulation, where each block consists of a number of subcarriers and subsymbols. The subcarriers are filtered with a filter prototype that shifts circularly in the time and frequency domains. This method can reduce out-of-band (OOB) emissions, make the spectrum efficient, and reduce inter-carrier interference (ICI) and inter-symbol interference (ISI). This GFDM block diagram is shown in Fig. 4.

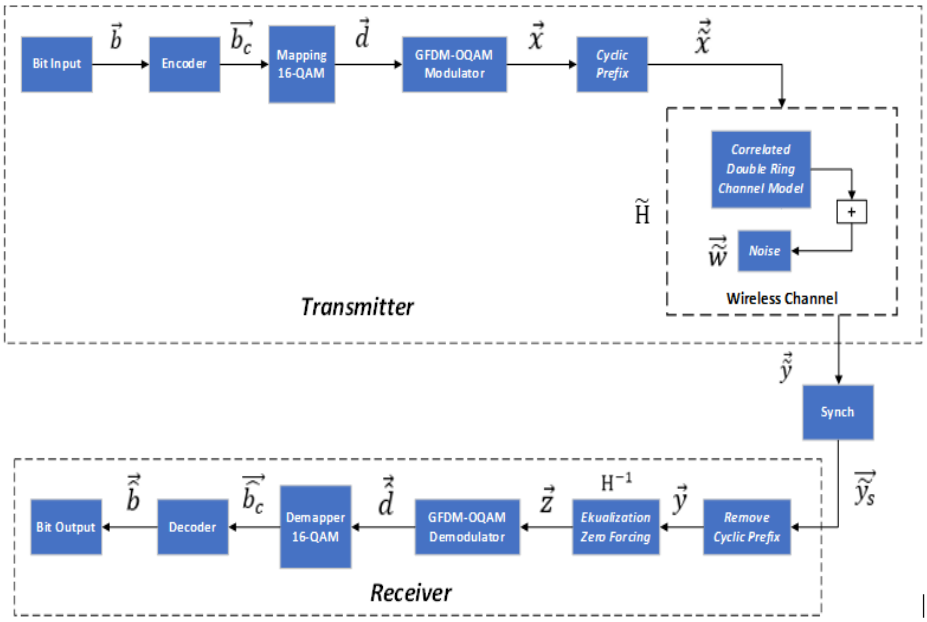

Figure 4. GFDM block diagram with the ZF equalizer.

Each parameter in the GFDM block diagram can be interpreted as follows:

$\vec{b}$ = The initial information sent is in the form of binary bits

$\overrightarrow{b_c}$ = Input bits from the mapper (the result of the conversion from bits to symbol that are integer values)

$\vec{d}$ = Block matrix from mapper results

$\vec{x}$ = Transmitted symbol

$\vec{\tilde{x}}$ = Symbols that have been added with cyclic prefix

$\tilde{\mathrm{H}}$ = Channel gain of CDR Rician Z(t)

$\vec{\tilde{w}}$ = Noise

$\vec{\tilde{y}}$ = Symbols that have undergone a multipath process and are exposed to Doppler shift

$\overrightarrow{\tilde{y}_s}$ = Accepted symbol but still has a cyclic prefix

$\vec{y}$ = Symbols that have been accepted and have removed the cyclic prefix

H^{-1} = Equalization process

$\vec{z}$ = Symbol of the output of the equalization

$\vec{\hat{d}}$ = Matrix output of the signal received by the GFDM demodulator

$\overrightarrow{\hat{b}_c}$ = The sequence of bits resulting from the demapper process (conversion from symbol to bit)

$\vec{\hat{b}}$ = The information received is in the form of bits

In Fig. 4, the binary data series $\vec{b}$ (conversion of analog signals to digital signals) generated by the data source is encoded as $\overrightarrow{\hat{b}_c}$. Data that has been encoded into a binary signal (bit) and will be mapped into a series of symbols in the mapper block. M-QAM modulation is used in this communication system, which is an M-ary QAM coding technique with the possible combinations of M different combinations consisting of n data bits. The result of the block mapper is the vector d, which mathematically can be written as $d = d_0, d_1, \ldots, d_{N-1}$, where N is the sum of all symbols. Then the vector will be converted into data and decomposed into GFDM blocks of size KxM in the GFDM modulator block, where K and M represent the number of subcarrier and subsymbol samples for each GFDM block. Furthermore, the decomposition vector can be written as $d = d_0, 0, d_1, 0, \ldots, d_{K-1}, M-1$. In this study, the simulation parameters are shown in Table II.

TABLE II. SIMULATION PARAMETERS

Parameter	Symbol	Value
Modulation type		16-QAM
Number of modulation level	m	4
Subcarrier	K	5
Subsymbol	M	9
Input bits	b	180180
Pulse shape filter	g	Root raised cosine
Roll-off factor	α	0.3
Carrier frequency	fc	5.8×10^9 Hz
Speed $V_1 = V_2$	V	5 m/s, 20 m/s, and 95 m/s
Departure angle between V_1 and scattering path	θ_n	Random (˚)
Arrival angle between V_2 and scattering path	Ψ_m	Random (˚)
Angle of distribution vehicle as transmitter	θ_{send}	45˚
Angle of distribution vehicle as receiver	θ_{31diff}	55˚
Number of scattering around T_X	N	8 or 16
Number of scattering around R_X	M	8 or 16
Channel models	H	Correlated double ring

The following formula is used to obtain the received signal equation, namely y(t), as shown in Fig. 3 [29]:

$$y(t) = x(t) \times h(t) + w(t) \quad (10)$$

where the value of $x(t)$ is the matrix of the output of the multi-carrier GFDM system.

D. The 16-QAM Modulation

The 16-QAM with guard interval and offset QAM (OQAM) with pulse shaping are the modulations used in this study. The difference between QAM and OQAM modulation is that in QAM, the Inphase bit position remains unchanged, whereas in OQAM, the bit shift occurs on the Quadrature side. We use the following equations to calculate the probability BER on the CDR channel for both Rayleigh and Rician properties of the GFDM-OQAM system [30]:

$$P_b, 16-QAM\ Rayleigh = \frac{3}{8}\left[1 - \frac{1}{\sqrt{1 + 5/(2\ x\ E_b/N_0)}}\right] \quad (11)$$

$$P_b, 16-QAM\ Rician = \frac{3}{8}\left[1 - \sqrt{\frac{E_b/N_0}{E_b/N_0 + 2}}\right] \quad (12)$$

E. Offset QAM (OQAM)

With the OQAM scheme, the spectrum of adjacent channels will overlap without causing crosstalk between subcarriers due to the half-symbol time delay between the in-phase and quadrature components of the signal on each subcarrier. Crosstalk is moved or shifted to even samples when complex symbols are transmitted from odd samples. This will reduce the effect of ICI because there is a reduction in the distance of adjacent channels on the subcarrier.

In OQAM modulation, the phase shift is limited to 0º and ± 90º every T second, unlike in QAM, where the phase jump is up to 180º. In contrast to QAM modulation, the I and Q channels in OQAM do not transition at the same time. This shows that the transition never exceeds 90º.

Fig. 5 is a block diagram of an OQAM demodulator with pulse shaping. From each channel, the real and imaginary parts are symbolized by $c_{k,n}$, then filtered by pulse shaping h(m) and h(m+N/2). These two parts are then summed and shifted to a predetermined frequency using baseband modulation [31]:

The output of the modulator is as follows [14]:

$$x(m) = \sum_{k=0}^{\infty} \sum_{n=0}^{N-1} [a_{k,n} h(m - kN) + j b_{k,n} h\left(m - kN + \frac{N}{2}\right)] e^{j\left(\frac{2\pi}{N} m + \frac{\pi}{2}\right) n} \quad (13)$$

From the above Eq. (13), we obtained [14]:

$$c_{k,n} = a_{k,n} + jb_{k,n} \quad (14)$$

where n is the number of samples per symbol interval and k is the number of channels.

In each channel, the received signal will be shifted back to its initial condition with baseband modulation and then re-filtered to separate the real and imaginary parts so that 1 sample per symbol is obtained [31]. The real part signal can be written as follows [31]:

$$a_{k,n} = \mathrm{Re}\{\sum_m h(m)x(kN-m)e^{j\left(\frac{2\pi}{N}m-\frac{\pi}{2}\right)n}\} \quad (15)$$

while the imaginary part signal can be written as follows [31]:

$$b_{k,n} = \mathrm{Im}\{\sum_m h\left(m-\frac{N}{2}\right)x(kN-m)e^{j\left(\frac{2\pi}{N}m-\frac{\pi}{2}\right)n}\} \quad (16)$$

F. Zero Forcing Equalizer

Zero forcing (ZF) equalizers have the least amount of complexity. This algorithm is used to set $\boldsymbol{H}$ as a communication channel matrix and $\boldsymbol{Y}$ as a matrix representing a linear process at the receiver so that the ZF meets the following requirements [25]:

$$YH = 1 \quad (17)$$

For each desired element of the symbol data to be detectable, it is necessary to have a process of forcing the parameters to zero value. This makes the $\boldsymbol{Y}$ matrix a pseudo-inverse (PI) matrix of the channel matrix $\boldsymbol{H}$, as shown in the following Eqs. (18-19) [25]:

$$Y_{ZF} = H^{-1} \; for \; N_{TX} = N_{RX} \quad (18)$$

$$Y_{ZF} = (H^H H)^{-1} H^H \; for \; N_{TX} \neq N_{RX} \quad (19)$$

where the value of N_{TX} and N_{RX} is the number of antennas on the transmitting and receiving sides.

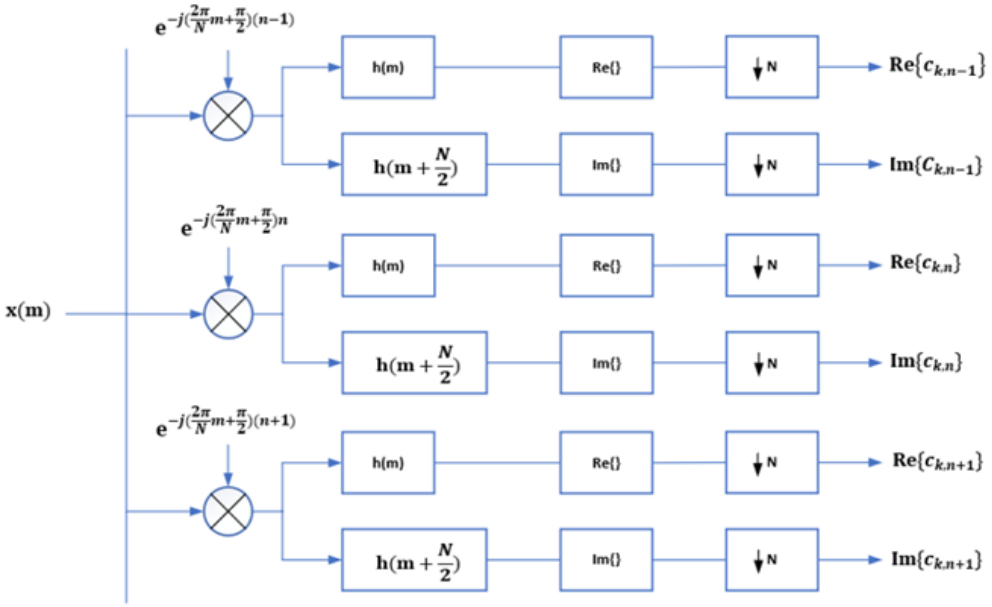

Figure 5. Block diagram of the OQAM demodulator.

III. Results and Discussion

This research is simulated using the simulation block diagram shown in Fig. 4 and the simulation parameters defined in Table II. The CDR channel parameters are established in accordance with the simulation settings detailed in Table I. This simulation's carrier frequency is 5.8 GHz, which refers to the frequency used in this simulation, using WAVE technology in the DSRC communication system [2]. As stated in Table III, the transmitter and receiver speeds on the CDR communication channel are adjusted to a low speed (5 m/s), a medium speed (20 m/s), and a high speed (95 m/s) to achieve the highest Doppler frequency at 1.6 kHz.

The information shown in Table III results in an analysis that the faster the speed on the transmitting and receiving sides, the greater the Doppler frequency (f_3) produced. The value of the Doppler frequency (f_3) obtained in this simulation is based on Eq. (4), which consists of parameter V_3 and wavelength.

TABLE III. Doppler Frequency For all Speed Scenarios

No	V_1 (m/s)	V_2 (m/s)	Angle θ_{send}	Angle θ_{31diff}	*Doppler Frequency* (Hz)
1	5	5	45°	55°	89.27
2	20	20	45°	55°	357.08
3	95	95	45°	55°	1696.2

The subsequent analysis is separated into two parts: the analysis of BER performance without ZF equalization and the analysis of BER performance with ZF equalization. Each of these scenarios is executed at three speeds, 5 m/s, 20 m/s, and 95 m/s, with two options for the number of scatterers, using 8 or 16 scatterers.

A. *Analysis of ZF Equalizer Performance with 8 Scatterers*

During this simulation, the performance of the system is observed without the ZF equalization procedure being executed. The received BER value is affected by the Doppler effect parameters and the multipath characteristics of the Rician CDR channel. The primary parameter noticed in this study is the BER value, which has a range of 15 dB for Eb/No. We adjusted the speed of the Rician CDR channel to 5 m/s, 20 m/s, and 95 m/s with 8 scatterers and a roll-off factor (RoF) of 0.3.

The simulation results are depicted in Fig. 6, which begins with a speed of 5 m/s and a minimal Eb/No value of 0 dB, yielding a BER value of 2.173×10^{-1}. However, when the Eb/No value is increased to its maximum of 15 dB, the BER value decreases to $1.688\text{x}10^{-1}$. Moreover, this also applies to the case of 20 m/s, where the BER value is 2.31×10^{-1} when the Eb/No value is the minimum and 1.853×10^{-1} when it is the maximum. For the situation with a velocity of 95 m/s, when the Eb/No value is 0 dB, the BER value is 2.359×10^{-1}. However, when the Eb/No value is 15 dB, the BER value is $1.911\text{x}10^{-1}$.

According to these results, the nonlinearity of the Rician CDR channel has a complete impact on the BER value achieved without utilizing ZF equalization. When the transmitter and receiver speeds are the highest, the BER value is the lowest compared with the same point in the other two speed cases. We also compare these results with the BER probability value on the Rician channel with 16-QAM modulation, which is inferior to the BER value on Eq. (12). This indicates that the simulation results have not exceeded the Shannon limit accounting for the theoretical BER limit point.

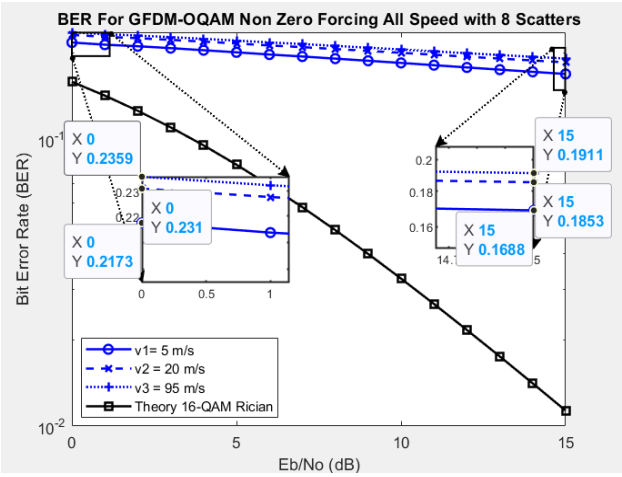

Figure 6. Comparison of Rician's CDR channel theory BER and GFDM-OQAM BER without ZF with 8 scatteres

Next, we recreate identical situations, as shown in Fig. 7, by incorporating the ZF method with reference to Eq. (17). When the CDR channel speed is set to 5 m/s and the Eb/No value is 0 dB, this simulation produces a BER value of $2.091\text{x}10^{-1}$. At the same time, a higher improvement in the BER value can be obtained by referring to Fig. 7. After equalizing ZF at the same speed for an Eb/No value of 15 dB, the BER value becomes $1.098\text{x}10^{-1}$ and it is better than the same position in Fig. 6. This may occur as a result of ZF equalization applied on the GFDM receiver side.

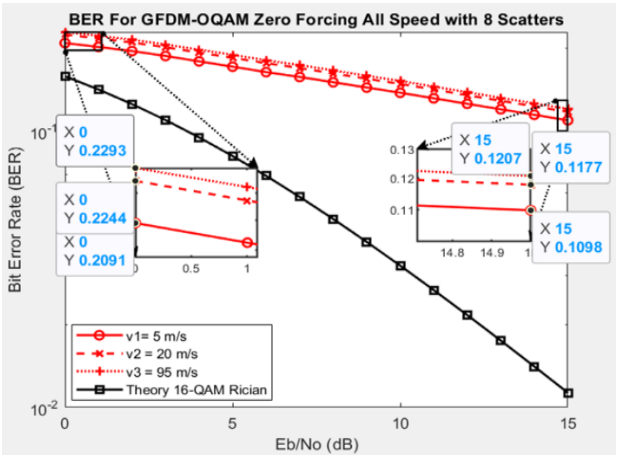

Figure 7. Comparison of Rician CDR channel theory BER and GFDM-OQAM BER after ZF process with 8 scatterers

In the following case, we can obtain results that are linear to what has occurred at 5 m/s. The results are summarized in Table IV. According to Table IV, the ZF equalization performance value yields the best results when the Eb/No value is the highest.

TABLE IV. COMPARISON OF BER VALUES BEFORE AND AFTER ZF EQUALIZATION WITH 8 SCATTERERS

	5 m/s		20 m/s		95 m/s	
Eb/No (dB)	0	15	0	15	0	15
BER Before ZF	0.209	0.109	0.224	0.117	0.229	0.120
BER After ZF	0.217	0.168	0.231	0.185	0.235	0.191

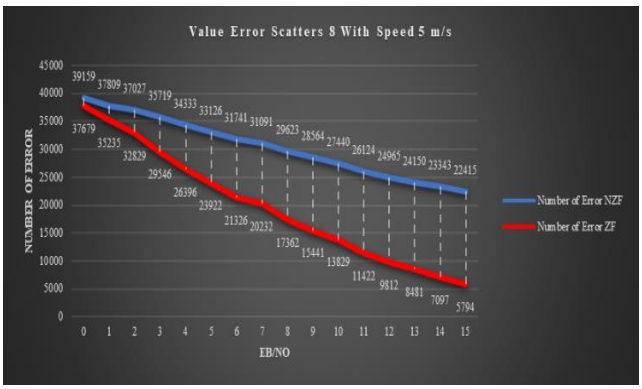

Figure 8. Comparison of number of error bits before and after ZF with 8 scatterers at speed of 5 m/s.

If it relates to the number of 180180 input bits sent into the GFDM block diagram, the number of bits determined

to be an error on the receiving side can also be evaluated. As indicated in Fig. 8, we have recapitulated the comparison between the number of error bits when the system was left without ZF and after it was equalized with ZF. At an EB/No value of 15 dB, ZF equalization results in fewer error bits, which are 5,794 as opposed to 22,415 when ZF equalization is not used. This indicates that the ZF equalization system can reduce error bits.

B. Analysis of ZF Equalizer Performance Results with 16 Scatterers

In this part, the effect of increasing the number of scatterers on the Rician CDR channel is analyzed by increasing the number of scatterers to 16 while maintaining the low-speed, medium-speed, and high-speed scenarios. As shown in Figs. 9-10, we compare the BER performance before and after ZF equalization, as applied for 8 and 16 scatterers.

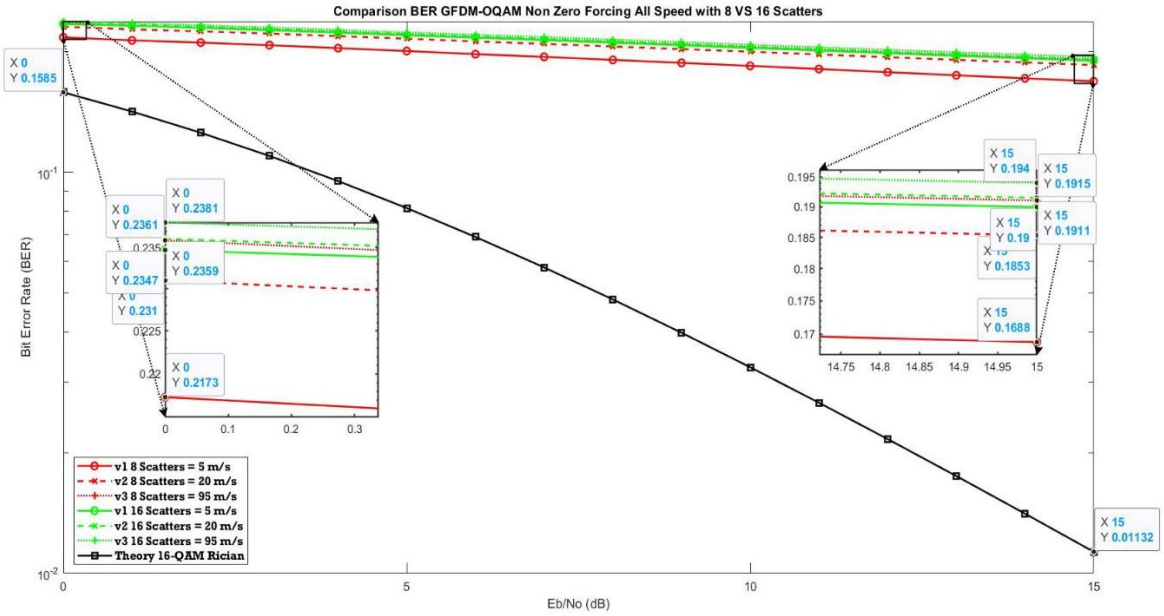

Figure 9. BER comparison of non-ZF with number of scatterers: 8 and 16.

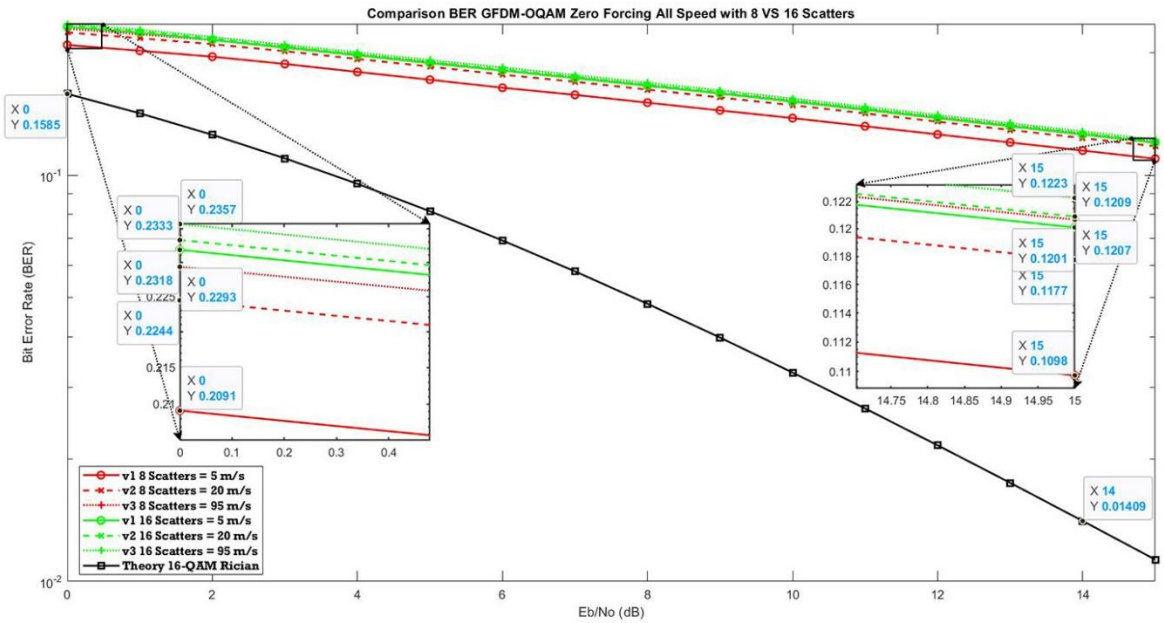

Figure 10. BER comparison without ZF with 8 and 16 scatterers

In Fig. 10, the BER values with 16 scatterers are all inferior to the BER values with 8 scatterers in every speed scenario. Even without ZF equalization, the pattern of BER value changes on the Rician CDR channel is linear with regard to BER and the number of scatterers, as shown by these results. All of these BER values are still lower

than the theoretical BER of 16-QAM on the Rician Fading channel, which takes Shannon's theory into consideration.

Table V provides a summary of BER performance under two conditions: without ZF equalization and with ZF equalization. The ZF equalization's effectiveness value contributes to an increase in BER performance at 95 m/s and 15 dB Eb/No. This is significantly better than the ZF equalization performance on the identical system with only eight scatterers.

TABLE V. COMPARISON OF BER VALUES BEFORE AND AFTER ZF WITH 16 SCATTERERS

	5 m/s		20 m/s		95 m/s	
Eb/No (dB)	0	15	0	15	0	15
BER Before ZF	0.235	0.19	0.236	0.192	0.238	0.194
BER After ZF	0.232	0.12	0.233	0.121	0.236	0.122

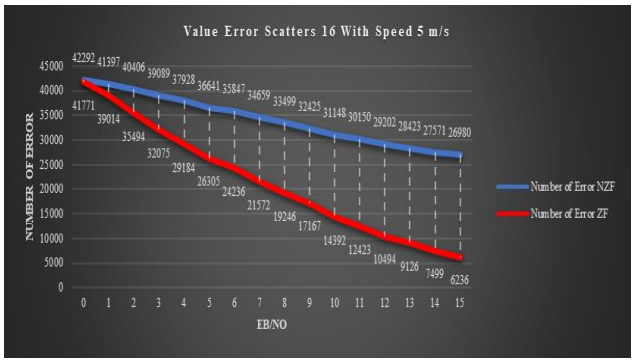

Figure 11. Comparison of the number of error bits before and after ZF with scatterer 8 at a speed of 5 m/s.

As illustrated in Fig. 11, the same study is conducted by comparing the number of error bits received when the system is left without ZF equalization and after ZF equalization is applied with the number of scatterers increased to 16. At a pace of 5 m/s, 26,980 bits received from 180,180 bits transmitted contain errors. This quantity of received bits bypasses the ZF equalization technique. At the same Eb/No value of 15 dB, the number of error bits received drops to 6,326 bits. Compared to the identical scenario with a fewer scatterer of 8 scatterers, the performance of this scenario with 16 scatterers is better. This demonstrates that the ZF algorithm is capable of overcoming the number of multipaths and the Doppler effect in mobile wireless communication channels.

II. CONCLUSION

This work provided a ZF equalization strategy for a Rician CDR channel using a GFDM multicarrier system. Prior to the ZF equalization procedure, the Rician CDR channel has a significant Doppler frequency and produces a linear BER value with changes in speed. At a high speed of 95 m/s with 8 scatterers, the ZF equalization proposed in this work proved effective in improving the BER performance. Regarding overcoming the multipath effect on the Rician CDR channel, increasing the number of multipaths has a linear influence on the BER value produced by the communication system in the absence of the ZF equalization procedure. We provide a ZF equalization method to counteract the rise in multipath to 16, resulting in an improvement in BER performance at a high speed of 95 m/s. On the basis of these results, it can be stated that the ZF equalization scheme presented in this study is capable of effectively overcoming the very strong Doppler effect on the Rician CDR channel as well as the multipath fading effect.

CONFLICT OF INTEREST

The authors declare no conflicts of interest.

AUTHOR CONTRIBUTION

Haryadi Teguh Pribadi conducted the research through the supervision of Wahyu Pamungkas and Anggun Fitrian. Haryadi Teguh Pribadi make the coding and validated by Wahyu Pamungkas. Wahyu Pamungkas wrote the paper while Anggun Fitrian did the checking of the paper. All authors had approved the final version.

ACKNOWLEDGEMENT

This research was supported by Institut Teknologi Telkom Purwokerto as a part of the Telkom Foundation.

REFERENCES

[1] A. Chachich, V. Fessmann, J. Arnold, D. Thompson, W. Fehr, and S. Stasko, "DSRC-unlicensed Device Test plan To characterize the existing radio frequency signal environment," Washington DC, 2015.

[2] Y. Li, "An overview of the DSRC/WAVE technology," *Lect. Notes Inst. Comput. Sci. Soc. Telecommun. Eng. LNICST*, vol. 74, pp. 544–558, 2012.

[3] B. Li, S. M. Mirhashemi, X. Laurent, and J. Gao, "Wireless access for vehicular environments," 2008.

[4] I. Nathaniel, L. Tan, and K. Laberteaux, "Measurement and analysis of wireless channel impairments in DSRC vehicular communications," 2008.

[5] L. Cheng, B. E. Henty, D. D. Stancil, F. Bai, and P. Mudalige, "Mobile vehicle-to-vehicle narrow-band channel measurement and characterization of the 5.9 GHz Dedicated Short Range Communication (DSRC) frequency band," *IEEE J. Sel.* Areas *Commun.*, vol. 25, no. 8, pp. 1501–1516, 2007.

[6] L. Liang, H. Peng, G. Y. Li, and X. S. Shen, "Vehicular communications: A physical layer perspective," *IEEE Trans. Veh. Technol.*, pp. 1–13, 2017.

[7] H. Rakouth *et al.*, "V2X communication technology: Field experience and comparative analysis," in *Proc. FISITA 2012 World Automotive Congress*, pp. 113–129, 2012.

[8] S. Arslan and M. Saritas, "The Effects of OFDM Design Parameters on the V2X Communication Performance : A Survey," *Veh. Commun.*, 2017

[9] A. Festag, "Standards for vehicular communication — From IEEE 802.11p to 5G," *e i* Elektrotechnik *und Informationstechnik*, 2015.

[10] D. W. Matolak, "V2V communication channels : State of knowledge," *New Results, and What's Next*, pp. 1–2, 2013.

[11] P. K. Singh, S. K. Nandi, and S. Nandi, "A tutorial survey on vehicular communication state of the art, and future research directions," *Veh. Commun.*, vol. 18, p. 100164, 2019.

[12] W. Viriyasitavat, M. Boban, H. M. Tsai, and A. Vasilakos, "Vehicular communications: Survey and challenges of channel and propagation models," *IEEE Veh. Technol. Mag.*, vol. 10, no. 2, pp. 55–66, 2015.

[13] C. Campolo and A. Molinaro, *Vehicular Ad hoc Networks (VANET) Standards, Solutions, and* Research. Torino: Springer, 2014.
[14] B. Kihei, J. A. Copeland, and Y. Chang, "Vehicle-to-vehicle LOS large-scale doppler channel model using GSCM," in *Porc. 2017 IEEE 14th Int. Conf. Mob. Ad Hoc Sens. Syst.*, pp. 250–256, 2017.
[15] S. E. Carpenter, "Evaluating the accuracy of vehicular channel models in a large-scale DSRC test," 2017.
[16] L. C. Wang and Y. H. Cheng, "A statistical mobile-to-mobile rician fading channel model," 2005.
[17] L. C. Wang, W. C. Liu, and Y. H. Cheng, "Statistical analysis of a mobile-to-mobile Rician fading channel model," *IEEE Trans. Veh. Technol.*, vol. 58, no. 1, pp. 32–38, 2009.
[18] W. Pamungkas, T. Suryani, and W. Wirawan, "Correlated double ring channel model at high speed environment in vehicle to vehicle communications," in *Proc. 2018 International Conference on Information and Communications Technology (ICOIACT) Correlated*, 2018, pp. 601–606.
[19] A. Fitrian Isnawati, W. Pamungkas, J. Hendry, and T. Suryani, "Modeling of power spectral density using correlated double ring channel model with OFDM for high mobility user on vehicular network," 2018.
[20] N. Fitri Awaliyah, W. Pamungkas, and A. Fitrian Isnawati, "Modeling doppler spectrum of correlated double ring channel model for V2V communication," 2021.
[21] J. Hendry, A. Fitrian Isnawati, and W. Pamungkas, "Analysis of position angle of arrival in multipath fading channel using correlated double ring channel model for VANET communications," *J. Infotel*, vol. 10, no. 2, 2018.
[22] P. S. Bithas, K. Maliatsos, and A. G. Kanatas, "V2V communication systems under correlated double-rayleigh fading channels," *IEEE Veh. Technol. Conf.*, vol. 2016-July, no. 3, pp. 1–4, 2016.
[23] S. Sunkara and G. U. Bhargava, "BER analysis of translation invariant wavelet based orthogonal frequency division multiplexing system for 5G wireless communication networks," *Int. J. Intell. Eng. Syst.*, vol. 11, no. 6, pp. 292–299, 2018.
[24] W. Indah Sari, A. Fitrian Isnawati, and K. Ni'Amah, "Performance Analysis GFDM Using MMSE Equalization in Audio Transmission," in *Proc. 10th IEEE Int. Conf. Commun. Networks Satell. Comnetsat 2021*, pp. 141–145, 2021.
[25] E. N. O. Herawati, A. F. Isnawati, and K. Niamah, "Analysis of Gfdm-OQAM performance using zero forcing equalization," in *Proc. 10th IEEE Int. Conf. Commun. Networks Satell. Comnetsat 2021*, pp. 135–140, 2021,.
[26] S. Chen, G. Dai, and T. Yao, "Zero-forcing equalization for OFDM Systems over doubly-selective fading channels using frequency domain redundancy," *IEEE Trans. Consum. Electron.*, vol. 50, no. 4, pp. 1004–1008, 2004.
[27] A. Nakamura, K. Ishizu, K. Ohno, and M. Itami, "A study on complexity reduction of zero-forcing ICI cannceller in mobile reception of OFDM," in *Proc. ICCE 2010 - 2010 Dig. Tech. Pap. Int. Conf. Consum. Electron.*, pp. 121–122, 2010.
[28] A. Nakamura and M. Itami, "Zero — Forcing ICI canceller U sing iterative detection for mobile reception of OFDM," pp. 153–154, 2014.
[29] W. Pamungkas, J. Hendry, and W. M. Hadiansyah, "An improved spectral temporal average method for mitigating doppler effects in V2V communications," *Int. J. Veh. Inf. Commun. Syst.*, vol. 6, no. 3–4, pp. 317–335, 2021.
[30] J. K. Kim, M. Lee, K. I. Lee, K. W. Park, and K. S. Woo, *MATLAB / Simulink for Digital Communication*., 2009.
[31] A. Vahlin, N. Networks, and P. O. Box, "Efficient algorithms for modulation and demodulation in ofdm-systems," *IEEE Trans. Wirel. Commun.*, vol. 8, no. 6, 2003.